Supporting Information for:

Unveiling 3D Morphology of Multiscale Micro-Nano Silver Sintering for Advanced Electronics Manufacturing by Ptychographic X-ray Nano-Tomography

Yu-Chung Lin[1#], Xiaoyang Liu[1#], Kang-Wei Chou[2], Esther H. R. Tsai[3,5], Chonghang Zhao[1], Mirko Holler[3], Ana Diaz[3], Stanislas Petrash[, 2], Yu-chen Karen Chen-Wiegart*[, 1, 4]*

1 Department of Materials Science and Chemical Engineering, Stony Brook University, Stony Brook, NY, 11794, USA
2 Henkel Corporation, Bridgewater, NJ, 08807, USA
3 Paul Scherrer Institut, Forschungsstrasse 111, CH-5232 Villigen, Switzerland
4 National Synchrotron Light Source - II, Brookhaven National Laboratory, Upton, NY, 11973, USA
5 Center for Functional Nanomaterials, Brookhaven National Laboratory, Upton, NY 11973, USA

*Corresponding Authors: karen.chen-wiegart@stonybrook.edu; stan.petrash@henkel.com
[#] Joint first authors

Experimental Method

1.1 Sample preparation

With pressure-assisted sintering (Samples A-C), the specimen was placed on the hot plate at 130 ºC for 12 min. Afterwards, the sample was sintered under a 10 MPa pressure and the temperature was ramped to 250 ºC in 15 min with a ramping rate of 15 ºC/min from room temperature; the samples were sintered for 5 min at 250ºC. For the sample sintered without pressure-assistance (Sample D), the specimen was annealed also by ramping the temperature in 15 min from room temperature to 250ºC. However, sintering without pressure requires a longer time, i.e. 60 min. After the sintering process is completed, two of the samples were aged under accelerated condition at 250 ºC in air for 24 hours to test their durability. The samples were noted as gold (Au) vs. nAu (no Au) for testing metallization effects, P vs. nP (no pressure) for testing sintering conditions, and A vs. nA for testing the aging effects.

The pristine nano-silver (Ag) powders and the sintered nano-Ag structure are shown in Figure 6 B. The pristine nano-Ag powders are triangle in shape, with ~100 nm thickness and ~2 μm length. The shape is consistent with crystalline Ag nanoparticles[1]. To disperse the Ag nanoparticles, fatty acid was added as a dispersion agent. After sintering, the Ag powders became well-connected, forming a porous structure.

To prepare the samples for the PXCT study, the samples were milled into a cylinder with diameter 14-16 μm by FIB and then lifted-out and mounted to a sample pin specifically developed for the nanoscale scanning instrument used for PXCT [2] measurements following a procedure developed previously [3]. Figure. 6 C shows the sample preparation process after milling by FIB.

1.2 X-ray nano-tomography by ptychography and X-ray fluorescence microscopy

Ptychography [4] is a lensless coherent diffractive imaging method that, when combined with tomography, offers quantitative electron density and absorption tomograms with nanoscopic resolution [5, 6]. In this work, four tomograms were obtained through PXCT experiments carried out at the cSAXS beamline (X12SA) at the Swiss Light Source, Paul Scherrer Institute (PSI), Switzerland. A general description of each tomographic measurement is given as follows. Measurements were conducted in air and at room

temperature with an instrument that allows scanning nano-tomography with about 10 nm position accuracy, well suited for PXCT [8,9]. The experimental setup is illustrated in Figure 6 D.

A double crystal Si (111) monochromator was used to provide a monochromatic radiation of 8.7 keV. The illumination was defined by a 50 μm-diameter central stop, a 170 μm-diameter Fresnel zone plate (FZP) [7] with an outer zone width of 60 nm, and a 30 μm-diameter order sorting aperture. The FZP and the central stop were both fabricated at the Laboratory for Micro and Nanotechnology, PSI, Switzerland. The focal distance was 71 mm and the sample was placed a few millimeters downstream the focus to give an illumination of around 5 μm in diameter. The scanning points followed a Fermat spiral pattern[8] with an average step size of 0.6 μm over a field of view (FOV) of approximately 20 μm horizontally by 10 μm vertically. At each scanning position, a diffraction pattern was collected at 7.3 m downstream of the sample with an exposure time of 0.1 sec using a Pilatus 2M detector [9]. The number of photons incident on a sample was around 7×10^7 photons/μm^2 per projection.

Around 600 projections were taken from 0 to 180 with an angular step of 0.3 , taking approximately 18 hours per tomogram. Ptychographic reconstruction algorithms, including difference map [10] and maximum likelihood [11], were applied to reconstruct 2D projections. Areas of 300 × 300 pixels were used on the detector, giving reconstructed images with a pixel size of about 20 nm. Two-dimensional projections were aligned [12] to give 3D tomograms based on modified filtered back projection. The phase tomograms are quantitative and correspond to the electron density, as shown in Figure S1 [6]. Image resolution was estimated by Fourier shell correlation (FSC) [13] to be around 32 nm.

To examine the elemental composition, simultaneous ptychography and fluorescence scans were performed on sample A for a 2D projection. For the fluorescence analysis, a Ketek energy dispersive detector was placed close to the sample at about 90 degrees from the incident X-ray direction. Measurements were taken at 11.2 keV to cover the emission peaks of Au, Ag, and Cu. A FZP with 100 μm diameter was used and the sample-to-FZP distance was adjusted to give a 2-μm-diameter beam. The sample was

scanned by this illumination at a 0.4 μm step following a Cartesian grid and an exposure time of 0.1 sec. The FOV was 7 μm horizontally and 20 μm vertically. The Ag fluorescence image in Figure 2 was generated by a simple integration of the emission spectra at 2.998 keV with a width of around +/-0.25keV, corresponding to the Lα peak positions. The Cu fluorescence map shows the integrated intensity at 7.998 keV with a width of roughly +/-0.25keV, corresponding to the Kα peaks.

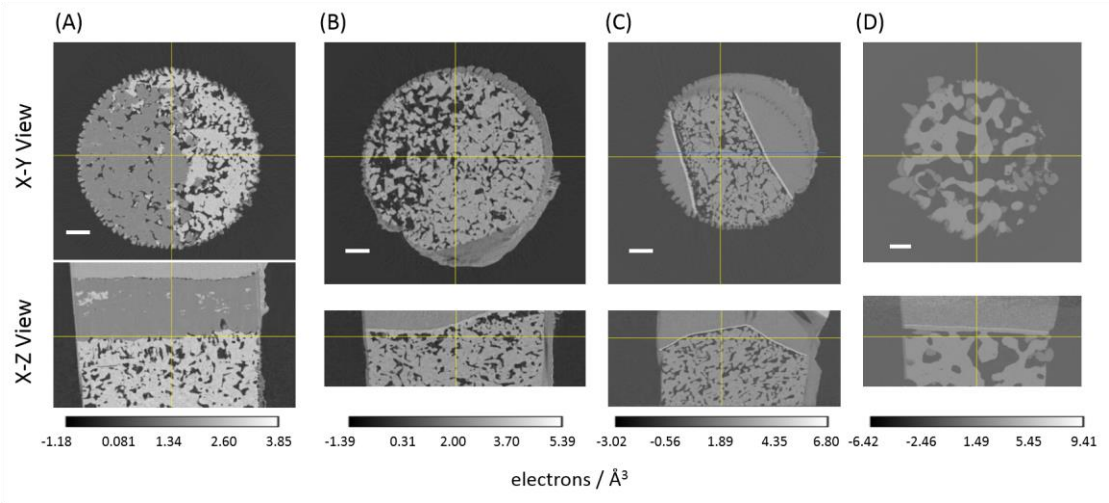

Figure S1 Reconstructed virtual cross section of the four Samples A-D from X-ray ptychographic tomography, with two different orthogonal views. Scale bars indicate 2 μm. Horizontal and vertical lines indicate the same planes for X-Y and XZ views.

1.3 Adhesion Performance Test

Evaluation of adhesion performance was conducted by performing 90° peel test using a peel test device from Frolyt GmbH (Freiberg, Germany). A peel speed of 8 mm/sec was used for all samples.

1.4 Three-dimensional morphological analysis

Quantitative morphology studies were performed directly on the measured 3D datasets, as has been previously done in other tomography studies using a transmission X-ray microscope [14]. In the following we describe the different aspects of this analysis in detail.

1.4.1 Segmentation

The central region in each of the 3D reconstruction image stack was cropped for further analysis. PXCT provides tomograms in which voxels have quantitative values of the

electron density of the sample, which for many light elements can be accurately converted to mass density [6]. Therefore, different materials in the sample can be segmented by their different densities and can be sometimes identified by their density values. The segmentation was conducted using Avizo software (FEI, Ver. 9.4). The phases including Cu, Cu oxide, Ni, Ag, Au and pore (air) were segmented directly using thresholding as their corresponding peaks in the histogram are well separated. For sample B (Au-P-A), as the Ag and Au peaks in the histogram overlap, the threshold value between Ag and Au phases was determined within a range where the slope of the histogram changes, indicating the mid-range of two overlapping peaks; while this process was semi-quantitative, within this range the morphological quantitative analysis results remain similar as the amount of Au is low. After the threshold value was determined, the artifacts of the threshold segmentation were examined by comparing the segmented images with the raw images and the segmented areas were corrected in Avizo. The 3D volume rendering was then conducted, and the segmented data were used for further 3D morphological quantification.

1.4.2 Phase distribution profile and feature size distribution

The various 3D morphological parameters were quantified using customized Matlab code developed in-house at Stony Brook University and Brookhaven National Laboratory. The phase distribution profiles of all phases were determined along the direction that is perpendicular to the interfaces. The distance was measured relative to the Ag-metal interface, which is defined as the zero position. The volume fraction of each phase at a given 2D plane was determined by voxel counting. The interface location was determined from the peak location of the first derivative of the Ag distribution profile. The feature size distribution of pore and Ag were obtained by well-established methods in the literature [15].

Average, standard deviation and full width half maximum (FWHM) of mean curvature of samples made at different conditions

Sample	Average (nm^{-1})	Median (nm^{-1})	Standard Deviation (nm^{-1})	FWHM (nm^{-1})
A: nAu-P-A	-0.00437	-0.05819	0.00649	0.01014
B: Au-P-A	-0.00461	-0.07517	0.00889	0.00789
C: Au-P-nA	-0.00245	-7E-07	0.00701	0.00822
D: Au-nP-nA	-3.5E-05	0.00314	0.00450	0.00355

Table S1 Average, standard deviation and full width half maximum (FWHM) of mean curvature of samples made at different conditions.

Reference

[1] S. H. Chen, D. L. Carroll, Nano Lett. **2002**, *2*, 1003.

[2] M. Holler, J. Raabe, R. Wepf, S. H. Shahmoradian, A. Diaz, B. Sarafimov, T. Lachat, H. Walther, M. Vitins, Rev. Sci. Instrum. **2017**, *88*, 113701.

[3] Y. C. K. Chen-Wiegart, F. E. Camino, J. Wang, ChemPhysChem **2014**, *15*, 1587.

[4] J. M. Rodenburg, A. C. Hurst, A. G. Cullis, B. R. Dobson, F. Pfeiffer, O. Bunk, C. David, K. Jefimovs, I. Johnson, Phys. Rev. Lett. **2007**, *98*, 034801; H. M. L. Faulkner, J. M. Rodenburg, Phys. Rev. Lett. **2004**, *93*, 4.

[5] M. Holler, M. Guizar-Sicairos, E. H. R. Tsai, R. Dinapoli, E. Muller, O. Bunk, J. Raabe, G. Aeppli, Nature **2017**, *543*, 402; M. Dierolf, A. Menzel, P. Thibault, P. Schneider, C. M. Kewish, R. Wepf, O. Bunk, F. Pfeiffer, Nature **2010**, *467*, 436.

[6] A. Diaz, P. Trtik, M. Guizar-Sicairos, A. Menzel, P. Thibault, O. Bunk, Phys. Rev. B **2012**, *85*, 020104(R).

[7] S. Gorelick, J. Vila-Comamala, V. A. Guzenko, R. Barrett, M. Salome, C. David, J. Synchrotron Radiat. 2011, 18, 442.

[8] X. J. Huang, H. F. Yan, R. Harder, Y. K. Hwu, I. K. Robinson, Y. S. Chu, Opt. Express **2014**, *22*, 12634.

[9] B. Henrich, A. Bergamaschi, C. Broennimann, R. Dinapoli, E. F. Eikenberry, I. Johnson, M. Kobas, P. Kraft, A. Mozzanica, B. Schmitt, Nucl. Instrum. Methods Phys. Res., Sect. A **2009**, *607*, 247.

[10] P. Thibault, M. Dierolf, A. Menzel, O. Bunk, C. David, F. Pfeiffer, Science **2008**, *321*, 379.

[11] M. Guizar-Sicairos, J. R. Fienup, Opt. Express **2008**, *16*, 7264; P. Thibault, M. Guizar-Sicairos, New J. Phys. **2012**, *14*, 063004.

[12] M. Guizar-Sicairos, A. Diaz, M. Holler, M. S. Lucas, A. Menzel, R. A. Wepf, O. Bunk, Opt. Express **2011**, *19*, 21345; M. Guizar-Sicairos, J. J. Boon, K. Mader, A. Diaz, A. Menzel, O. Bunk, Optica **2015**, *2*, 259.

[13] M. van Heel, M. Schatz, J. Struct. Biol. **2005**, *151*, 250.

[14] Y. C. K. Chen-Wiegart, P. Shearing, Q. X. Yuan, A. Tkachuk, J. Wang, Electrochem. Commun. **2012**, *21*, 58; Y. C. K. Chen-Wiegart, T. Wada, N. Butakov, X. H. Xiao, F. De Carlo, H. Kato, J. Wang, D. C. Dunand, E. Maire, J. Mater. Res. **2013**, *28*, 2444; Y. C. K. Chen-Wiegart, J. S. Cronin, Q. X. Yuan, K. J. Yakal-Kremski, S. A. Barnett, J. Wang, J. Power Sources **2012**, *218*, 348; Y. J. Liu, F. Meirer, C. M. Krest, S. Webb, B. M. Weckhuysen, Nat. Commun. **2016**, *7*; Y. C. K. Chen, Y. S. Chu, J. Yi, I. McNulty, Q. Shen, P. W. Voorhees, D. C. Dunand, Appl. Phys. Lett. **2010**, *96*; Y. J. Liu, F. Meirer, J. Y. Wang, G. Requena, P. Williams, J. Nelson, A. Mehta, J. C. Andrews, P. Pianetta, Anal. Bioanal. Chem. **2012**, *404*, 1297; G. J. Nelson, W. M. Harris, J. J. Lombardo, J. R. Izzo, W. K. S. Chiu, P. Tanasini, M. Cantoni, J. Van Herle, C. Comninellis, J. C. Andrews, Y. J. Liu, P. Pianetta, Y. S. Chu, Electrochem. Commun. **2011**, *13*, 586.

[15] J. Alkemper, P. W. Voorhees, Acta Mater. **2001**, *49*, 897; B. Munch, L. Holzer, J. Am. Ceram. Soc. **2008**, *91*, 4059; Y. C. K. Chen-Wiegart, S. Wang, Y. S. Chu, W. J. Liu, I. McNulty, P. W. Voorhees, D. C. Dunand, Acta Mater. **2012**, *60*, 4972.